

Paper Number: **663**

Title: **Influence of Mixed Mode I-Mode II Loading on Fatigue Delamination Growth Characteristics of a Graphite Epoxy Tape Laminate**

Authors :

James G. Ratcliffe

William M. Johnston Jr.

ABSTRACT

Mixed mode I-mode II interlaminar tests were conducted on IM7/8552 tape laminates using the mixed-mode bending test. Three mixed mode ratios, $G_{II}/G_T = 0.2$, 0.5, and 0.8, were considered. Tests were performed at all three mixed-mode ratios under quasi-static and cyclic loading conditions, where the former static tests were used to determine initial loading levels for the latter fatigue tests. Fatigue tests at each mixed-mode ratio were performed at four loading levels, G_{max} , equal to $0.5G_c$, $0.4G_c$, $0.3G_c$, and $0.2G_c$, where G_c is the interlaminar fracture toughness of the corresponding mixed-mode ratio at which a test was performed. All fatigue tests were performed using constant-amplitude load control and delamination growth was automatically documented using compliance solutions obtained from the corresponding quasi-static tests. Static fracture toughness data yielded a mixed-mode delamination criterion that exhibited monotonic increase in G_c with mixed-mode ratio, G_{II}/G_T . Fatigue delamination onset parameters varied monotonically with G_{II}/G_T , which was expected based on the fracture toughness data. Analysis of non-normalized data yielded a monotonic change in Paris law exponent with mode ratio. This was not the case when normalized data were analyzed. Fatigue data normalized by the static R-curve were most affected in specimens tested at $G_{II}/G_T = 0.2$ (this process has little influence on the other data). In this case, the normalized data yielded a higher delamination growth rate compared to the raw data for a given loading level. Overall, fiber bridging appeared to be the dominant mechanism, affecting delamination growth rates in specimens tested at different load levels and differing mixed-mode ratios.

INTRODUCTION

Delamination is a key damage mode exhibited by polymer matrix composite laminates [1-2]. Delamination is typically characterized based on linear elastic fracture mechanics (LEFM) using the strain energy release rate, G . This form of

James G. Ratcliffe Durability, Damage Tolerance, and Reliability Branch, NASA Langley Research Center, Hampton, VA 23681, U.S.A.
William M. Johnston, STC (Science and Technology Corporation), 21 Enterprise Parkway, Suit 150, Hampton, VA 23666, U.S.A.

characterization is favored over stress intensity factor, K , due to the difficulty in determining the stress field associated with K in heterogeneous material systems such as laminated composites [3-4].

Several testing methods have been proposed for determining the quasi-static critical strain energy release rate, G_c , under opening (Mode I), in-plane shear (Mode II), scissoring shear (Mode III), and mixed-mode I/II loading conditions. These efforts have led to the development of internationally recognized testing standards [5-8].

Many of these testing methods have been, or are in the process of being, extended to account for fatigue loading conditions. In general, fatigue data are interpreted separately in two ways. In the first case, growth onset due to fatigue loading of an existing delamination is characterized in a manner loosely analogous to S-N characterization of metal fatigue. Here, strain energy release rate is determined as a function of cycles necessary for delamination growth onset, N , yielding a G - N curve. This characterization method for mode-I delamination is available as an ASTM International testing standard [9]. The second case involves characterization of fatigue delamination growth rate in a manner analogous to the Paris law relationship utilized for characterizing metal fatigue crack growth rates. In this case, rather than determining growth rate, da/dN , as a function of K , delamination growth rates are typically determined using G . The linear portion of log-log plot of da/dN versus G is generally identified and determined to be equivalent to a Paris law, where growth rate is defined as $da/dN=DG^n$ (D and n being constants associated with the material in question).

The above methods have been applied to characterizing fatigue delamination growth in several different material systems under mode ratios ranging from pure mode I to pure mode II [10-15]. A considerable amount of work has also been conducted to develop laws for mixed-mode I/II fatigue delamination growth rates, where the Paris law is generalized to account for mixed-mode ratio effects [16-19]. However, these studies, in general, offer little consensus on a correct form of a mixed-mode fatigue law that would apply to any material system. Theoretically, if G_{IIc} is always greater than G_{Ic} for a given material system, then it may be argued that the Paris law constants, D and n , should monotonically change with mixed-mode ratio, G_{II}/G_I . Although in some instances this has been shown to be the case [18], other work has shown that the Paris law constants vary with G_{II}/G_I non-monotonically [17].

The objective of the current work was to characterize fatigue delamination growth rates in IM7/8552 graphite/epoxy at three mixed-mode I/II ratios, $G_{II}/G_I=0.2, 0.5,$ and 0.8 . This work was conducted in concert with separate studies on the same material system (same material spec and manufacturer) in which fatigue delamination growth rates under pure mode I and mode II loading conditions were determined [20, 21]. Details of the material, test specimens, procedures and results/discussion are presented in what follows.

EXPERIMENTAL PROCEDURES

Materials and specimens

A single manufacturer denoted as Source 1 in Refs. 20 and 21 supplied mixed-mode bending (MMB) specimens made of IM7/8552 graphite/epoxy tape.

A schematic of an MMB specimen is given in Figure 1(a). Each specimen consisted of a 24-ply unidirectional, laminated beam, nominally 0.18-inch thick, 1-inch wide, and 7-inches long. Specimens contained a 2-inch long, 5×10^{-3} -inch thick polytetrafluoroethylene (PTFE) insert at the midplane at one end to act as an artificial delamination, as illustrated in Figure 1(a). Piano hinges were bonded to each side of the delaminated portion of every specimen using a 2-part epoxy adhesive paste (Hysol EA 9259.3), which was cured at 300°F for one hour. This resulted in a nominal delamination length, a_0 , of 1 inch as illustrated in Figure 1(a). Immediately prior to testing, the edges of each specimen were coated with a thin layer of white paint and marked in 0.05-inch increments, starting from the tip of the insert to a length of 1 inch.

Mixed-Mode Bending (MMB) Test

All specimens were tested according to the MMB test procedure detailed in ASTM International testing standard, D6671 [6] (referred to as D6671 in the remainder of this paper). The MMB test involves a combination of the loading conditions of the double cantilever beam (DCB) and end-notch flexure (ENF) tests [5, 8]. A schematic of an MMB specimen and its loading fixture is presented in Figure 1(b). The specimen sits on a support roller on the fixture base, and the piano hinges are clamped to the base and loading lever (see Figure 1(b)). The location of applied load, P , (see Figure 1(b)) on the loading lever is adjustable. By changing horizontal distance, c_L , between this load-application point and the upper roller (also referred to as the lever length, Figure 1(b)), the mixed-mode I/II ratio applied to a specimen can be varied. For example, a lever length equal to zero (load-application point, P , coincident with upper roller) yields a pure mode-II form of loading at the delamination front of a specimen (although the MMB test in this configuration has not generally been employed for mode II delamination characterization).

Conversely, theoretically an infinite lever length will yield pure mode-I loading conditions. A picture of an MMB specimen positioned within the MMB loading fixture for all static and fatigue testing is presented in Figure 2. Realistically, G_{II}/G_I can vary between 0.2 and 0.8.

Closed-form solutions of the mode-I and mode-II strain energy release rate components for the MMB specimen are used to determine the lever length necessary for a specified mixed-mode I/II ratio. These equations are also used for reducing the test data in order to calculate G_c for a given mixed-mode ratio, as discussed later in this section.

Three mixed-mode ratios, $G_{II}/G_I=0.2, 0.5,$ and 0.8 (corresponding to lever lengths of 3.66, 1.63, and 1.07 inches, respectively), were considered in both static and fatigue tests conducted in the current study. Details of the static and fatigue test procedures and data reduction methods are given in what follows.

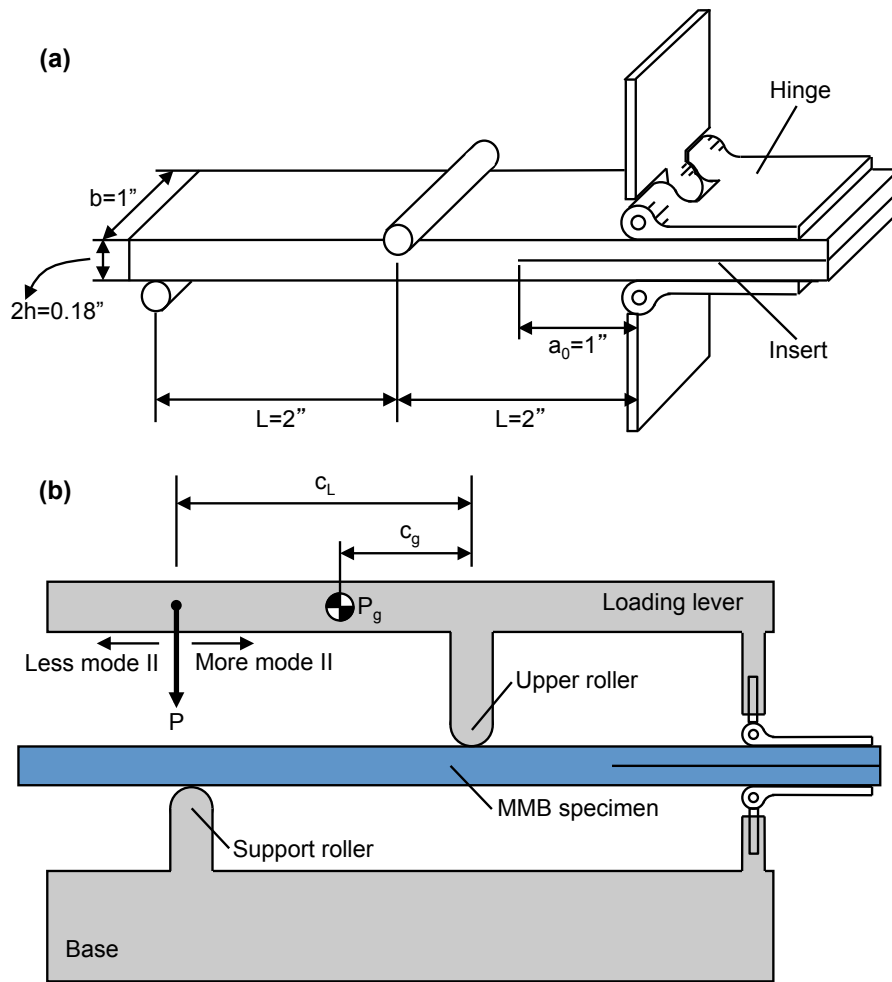


Figure 1. (a) MMB specimen (not to scale and all dimensions nominal). (b) MMB test fixture.

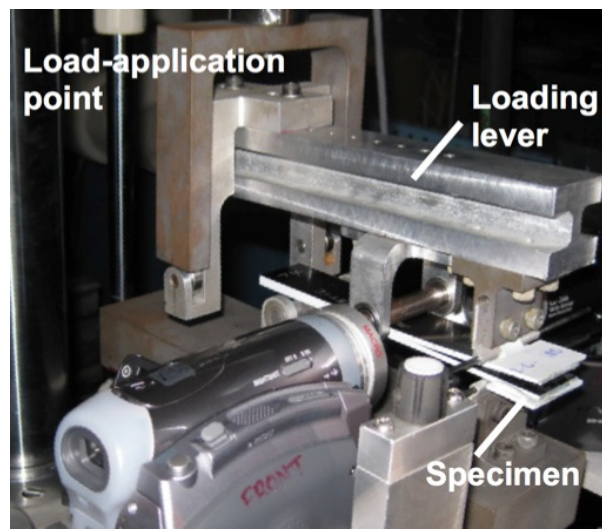


Figure 2. MMB test setup.

Static MMB Test procedure

Static MMB tests were conducted using a 5 kip servo-hydraulic test machine equipped with a 250-lbf load cell. Specimens loaded at mixed-mode ratios of $G_{II}/G_T = 0.5$ and 0.8 were precracked (PC) prior to fracture testing and the resulting fracture toughness values were compared with those from non-precracked (NPC) specimens. Specimens tested at $G_{II}/G_T = 0.2$ were not precracked due to the concern that fiber bridging may develop, yielding erroneous initiation fracture toughness measurements. Each specimen was precracked at the mixed-mode ratio to be performed during the actual fracture test. In these cases, an approximately 0.12 inch precrack was grown quasi-statically in the specimens. Specimens were loaded in displacement control at a rate of 0.05 inches per minute. Critical force values associated with delamination initiation and subsequent propagation at approximately 0.05-inch increments of delamination growth were recorded. Specimens were unloaded at the same rate after approximately 0.8 inches of delamination growth had occurred. Specimen force-displacement response was recorded for the entire duration of a test using a sample rate of one data point per second. Critical strain energy release rates for delamination initiation and propagation were calculated using the method described in the data reduction section. Six NPC specimens were tested at $G_{II}/G_T=0.2$. At $G_{II}/G_T=0.5$ and 0.8 , six specimens each were tested with and without precracks, resulting in a total of 30 static tests.

Fatigue MMB Test procedure

The same loading fixture used for static tests (Figure 2) was used to perform all fatigue testing. Specimens were subjected to sinusoidal cyclic loading at a frequency of 3Hz. This is slightly lower than the 5Hz frequency used in companion studies of mode-I and mode-II delamination [20, 21], and was selected to avoid unwanted dynamic effects from the relatively massive MMB loading lever. In previous work concerning mode-I and mode-II delamination of graphite/epoxy laminates, mild changes in growth rates with test frequency ranging between 1 and 5Hz were reported [22]. Therefore, the slight difference in frequency used for the current tests was assumed to not significantly affect delamination growth rates. Tests were conducted in load control using a commercially available software for data accumulation and retrieval [23]. Tests were run at maximum cyclic loads, P_{max} , corresponding to initial G_{max} values approximately equal to 60%, 50%, 40%, and 30% of the average value of G_C from fracture tests for a given mixed-mode ratio. Using D6671 [6], G_{max} is given by:

$$G_{max} = \frac{12[P(3c-L) + P_g(3c_g - L)]^2}{16b^2h^3L^2E_{1f}}(a + \chi h)^2 + \frac{9[P(c+L) + P_g(c_g + L)]^2}{16b^2h^3L^2E_{1f}}(a + 0.42\chi h)^2 \quad (1)$$

Rearrangement of Equation (1) yields an expression for P_{max} corresponding to a given G_{max} value:

$$P_{max} = \frac{\sqrt[4]{3}\sqrt{G_{max}b^2h^3L^2E_{1f}} - P_g[(a + \chi h)(3c_g - L) + \sqrt{3/4}(a + 0.42\chi h)(c_g + L)]}{(a + \chi h)(3c - L) + \sqrt{3/4}(a + 0.42\chi h)(c + L)} \quad (2)$$

where b , h , and L , and a are the specimen dimensions in Figure 1(a). The terms c , P_g , C_g are the lever arm length, loading lever weight, and center of gravity location, respectively, shown in Figure 1(b). The flexural modulus, E_{If} is computed using a closed-form solution in D6671 based on data from the static tests. The parameter χ is a crack length correction factor [6]:

$$\chi = \sqrt{\frac{E_{11}}{11G_{13}} \left\{ 3 - 2 \left(\frac{\Gamma}{1+\Gamma} \right)^2 \right\}}, \quad \Gamma = 1.18 \sqrt{\frac{E_{11}E_{22}}{G_{13}}} \quad (3)$$

The engineering properties E_{11} , E_{22} , and G_{13} used in the above equation are given in Ref. [24].

During fatigue, specimen compliance was measured every two cycles until the test was stopped. The commercial software system monitored compliance and estimated a corresponding crack length using a specimen compliance solution based on static test data. The system stopped cycling when the estimated crack length reached 0.8 inches. After unloading, the specimens were pried open to allow measurement of the initial and final delamination length and front shapes. Data reduction software was developed for computing cyclic G levels and delamination growth rates from the compliance/cycle count data collected during a test. This procedure was used for tests conducted at all three mixed-mode ratios. Four repeat tests were conducted for each loading level at each mode ratio resulting in a total of 48 fatigue tests.

Data Reduction

Data from the static tests were reduced to determine fracture toughness values and static R-curves for each mixed-mode ratio. These data were also used to establish loading levels at the start of a fatigue test. Fatigue test data were used to determine delamination onset and growth curves for each mixed-mode ratio.

STATIC TESTS

Closed-form solutions for lever length, c , required for a given mixed-mode ratio: G_{II}/G_T , and the total strain energy release rate, G_T , at delamination growth initiation and subsequent propagation are presented in Ref. 6 and used in this study. The value of G_T at delamination growth initiation is assumed to be equivalent to the fracture toughness, G_c , corresponding to each of the three mixed-mode ratios in question. In all cases, initiation G_c was computed using Equation 1 with $P=P_{max}$. Static R-curves were generated for each mode ratio based on the delamination propagation data. Specimen flexural modulus, E_{If} , of each specimen was also computed using a closed-form solution from Ref. 6.

FATIGUE TESTS

The FTA data acquisition system used for the fatigue tests provided a record of specimen compliance as a function of cycle count for the duration of each test at a sample rate of once every two cycles. These compliance data were analyzed to

determine corresponding delamination length values using the following expression from D6671 [6]:

$$C = \frac{\delta}{P} = (8bE_{11}h^3L^2)^{-1} \left[4(3c-L)^2 (a+h\chi)^3 + (c+L)^2 (2L^3 + 3(a+0.42h\chi)^3) \right] \quad (4)$$

Rearrangement of Equation 4 yields the expression used to calculate delamination length, a :

$$a = \frac{\sqrt[3]{8CbE_{11}h^3L^2} - \sqrt[3]{2L^3(c+L)^2} - h\chi \left(\sqrt[3]{4(3c-L)^2} + 0.42\sqrt[3]{3(c+L)^2} \right)}{\sqrt[3]{4(3c-L)^2} + \sqrt[3]{3(c+L)^2}} \quad (5)$$

The raw compliance data were initially applied to Equation 5 yielding a corresponding delamination length every two cycles. Delamination growth increments at this sample rate were significantly affected by the noise in the raw (compliance) data. Consequently, the compliance data were parsed to remove delamination growth intervals less than 0.004 inches, which was approximately three times the noise level of the raw test data. A comparison of parsed and raw data corresponding to the first 8000 cycles of a fatigue test conducted with a mixed-mode ratio $G_{II}/G_I=0.5$ and $G_{max}=0.5G_c$ is presented in Figure 3(a). An example of the entire parsed data from the same test is given in Figure 3(b). These parsed data were analyzed to compute G_{max} as a function of delamination growth rate, da/dN , using the methods described in what follows.

Fatigue delamination growth rate, da/dN , was calculated from the parsed data using the secant and the incremental polynomial methods, described in ASTM E647 [25]. Using the secant method, fatigue crack growth rate was calculated as:

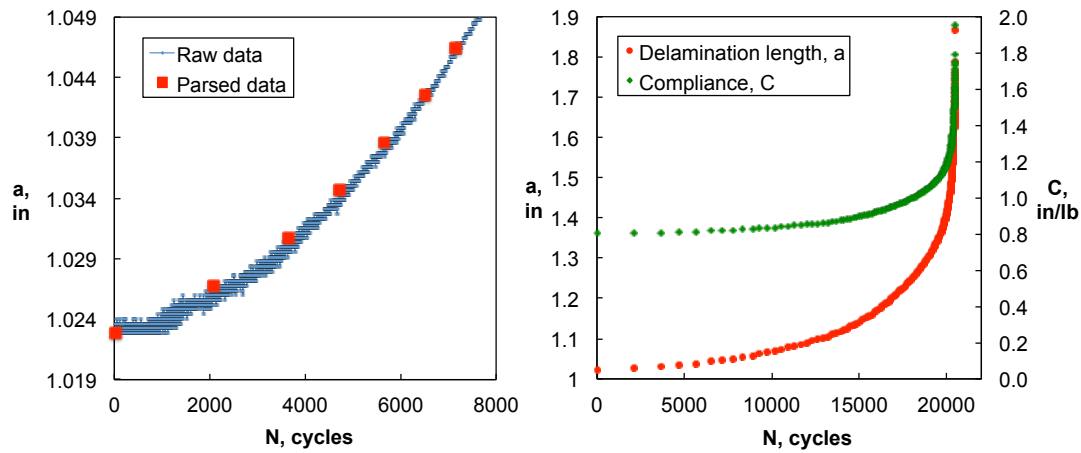
$$\frac{da}{dN} = \frac{a_{i+1} - a_i}{N_{i+1} - N_i} \quad (6)$$

where a_i is a crack length corresponding to cycle count N_i , and a_{i+1} and N_{i+1} are crack length and cycle count values corresponding to the next available data point. The crack length used to calculate G from this two-point linear fit method is taken as the midpoint (average a) of the delamination growth increment. Alternatively, the incremental polynomial method can be used to help reduce error induced by noisy experimental data. The incremental polynomial method fits a parabola to successive sets of seven points of data. The fatigue delamination growth rate is calculated as the derivative of this fit evaluated at the center point. The delamination length used to calculate G is also taken from the center of the fit. The maximum cyclic G level was determined by substituting the estimated crack length (Equation 5) and cyclic load for each growth rate measurement into Equation 1. The data were plotted in the typical log-log form used for Paris law crack growth [26]. Typical results for fatigue delamination growth are shown in Figure 4(a) for the secant (2-point fit) and the incremental polynomial (7-point fit) data. The incremental polynomial method resulted in significantly lower noise in the reduced data and was thus used to reduce all fatigue data in the current work.

The fatigue data shown in Figure 4(a) correspond to a complete test involving approximately 0.8 inches of delamination growth and is representative of data obtained from all fatigue tests. As illustrated in Figure 4(a), the data exhibit a linear region to which a Paris law of the following form was fit:

$$\frac{da}{dN} = DG_{\max}^n \quad (7)$$

Fiber bridging that is very likely present during MMB tests is thought to artificially reduce delamination growth rates, yielding non-conservative estimates. A method was adopted that attempts to account for this effect, which involves normalization of the fatigue data by the static R-curve [27, 28]. This involves determining the critical strain energy release rate, G_R , as a function of delamination extension using the static test data. The loading level, G_{\max} , at each stage of a fatigue test is then normalized by its corresponding value of G_R (corresponding to the same delamination extension). The normalized data are also multiplied by the fracture toughness (for the mixed-mode ratio in question) in order to provide a meaningful comparison with raw fatigue data. An example of normalized and raw data from a fatigue test with $G_{II}/G_I=0.2$ is presented in Figure 4(b).



(a) Parsed versus complete data (b) Parsed compliance and calculated delamination length

Figure 3 Parsed and complete data sets.

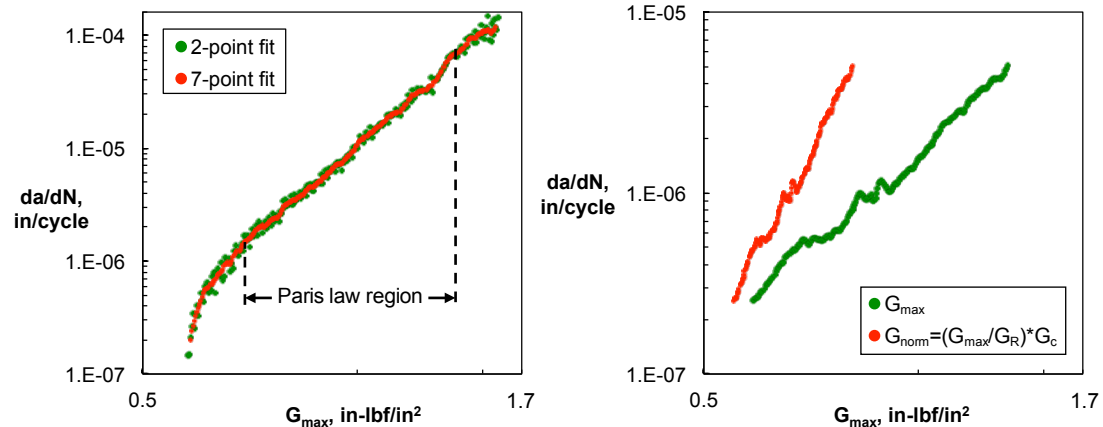


Figure 4 (a) Fatigue data from both ASTM E647 methods. (b) Normalized and raw fatigue data.

This normalization procedure was adopted in a companion study on mode-I delamination [20] with results similar to those presented in Figure 4(b). This procedure assumes that static R-curves arise primarily from fiber bridging, and also assumes that the extent of fiber bridging in a fatigue test is equivalent to that of a static test. The latter assumption may be invalid due to the different amounts of opening displacement applied during static and fatigue testing. However, a recent study on mode-I delamination indicated that the latter assumption may well be valid [29]. However, the method is used here to provide consistency in comparison of the data. Fatigue delamination onset was also recorded in each test. Delamination onset was assumed to occur when specimen compliance had increased by 5% over its original value [9].

RESULTS AND DISCUSSION

Static Tests

The force-displacement response of specimens loaded at the three mixed-mode ratios is presented in Figure 5(a). The response of duplicate specimens for all mixed-mode ratios exhibited a high repeatability and so only a single example of each is shown in Figure 5(a) for brevity. Specimens tested at mixed-mode ratios of $G_{II}/G_T=0.5$ and 0.8 were precracked, and those tested at $G_{II}/G_T=0.2$ were not precracked. Overall, specimen response was linear up to delamination initiation and propagation, followed by linear unloading. As expected, delamination growth was more unstable in specimens tested at higher mode II mixed-mode ratios, G_{II}/G_T . The red circles on each response plot indicate moments where delamination initiation and propagation were visually observed. Yellow and green circles indicate the deviation from linearity, P_{NL} and the maximum force, P_{max} , respectively. In general, specimen response deviated from linearity earlier in the loading stage in specimens tested at higher mode II mixed-mode ratios, G_{II}/G_T .

Average values of G_c corresponding to delamination growth initiation (based on $P=P_{max}$ in Equation 1) are plotted in Figure 5(a) as a function of G_{II}/G_T and summarized in Table I. Data from tests conducted on non-precracked (NPC) and precracked (PC) specimens are included in the figure. These data are combined with G_{Ic} and G_{IIc} reported in the two companion studies [20, 21] to form a mixed-mode delamination initiation criterion in the range, $0 < G_{II}/G_T < 1$. Scatter in the data was reasonably small, with coefficients of variation (CoV) not exceeding 13% for all tests conducted and less than 8% in data based on PC tests. In all cases, G_c from PC specimens is lower than G_c from NPC specimens, and this difference increases as the mode II component of G increases. This is consistent with findings from a recent round-robin study of the ENF test in which PC specimens were reported to yield significantly lower values of G_{IIc} for graphite/epoxy and glass/epoxy laminates (G800-9736 and S4/8552-1) compared to values from NPC specimens [30]. The explanation for this may be that less work is required to initiate delamination in PC specimens because the fracture process zone known to correspond to mode-II delamination [31], is already present in PC specimens, but not in pristine NPC specimens. This effect manifests itself in the current data as an increasing difference

between NPC and PC-based toughness values as G_{II}/G_T is increased. The data were also fit to the following mixed-mode delamination criterion (referred to as BK) [16]:

$$G_c = G_{Ic} + (G_{IIc} - G_{Ic}) \left(\frac{G_{II}}{G_T} \right)^\eta \quad (8)$$

This yielded the solid lines shown in Figure 5(b). The upper solid line in Figure 5(b) corresponds to application of Equation 8 to G_{Ic} and NPC-based G_{IIc} from the two companion studies. The lower solid line is based on G_{Ic} and PC-based G_{IIc} from the companion studies. Note that no precracking was performed in the companion study on mode-I delamination and thus only one value of G_{Ic} is used here. An exponent of $\eta=2.1$, was employed in both of the above cases, resulting in relationships that exhibit reasonable comparison to the experimental data.

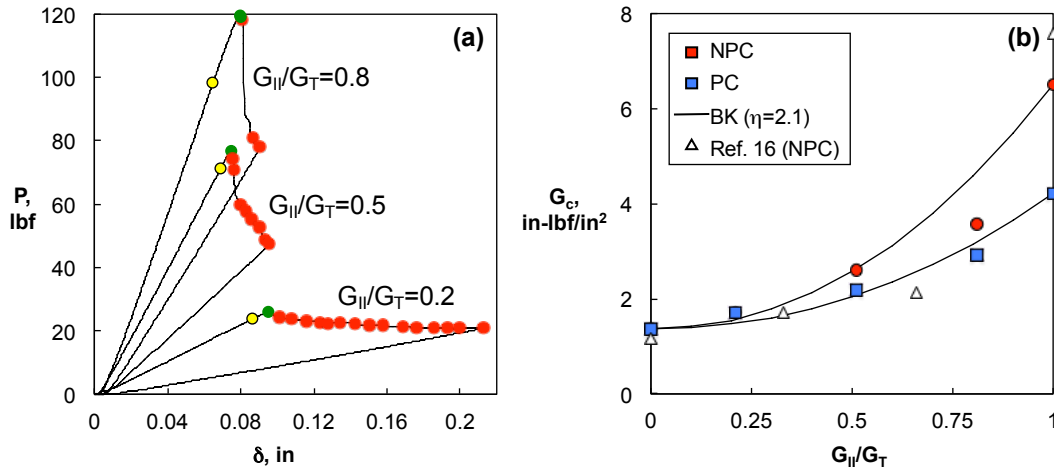


Figure 5 (a) Sample force-displacement responses at each mixed-mode ratio. (b) Mixed-mode delamination initiation criteria.

TABLE I. Non-precrack (NPC) and precrack (PC) mixed-mode fracture toughness.

G_{II}/G_T	0 [21]	0.2	0.5	0.8	1.0 [20]
NPC G_c , in-lbf/in ² (CoV, %)	1.37	1.71 (5.7)	2.60 (13.2)	3.56 (5.4)	6.50 (6.5)
PC G_c , in-lbf/in ² (CoV, %)	N/A	N/A	2.17 (5.9)	2.93 (6.7)	4.22 (7.6)

Fracture toughness values reported previously for IM7/8552 [15] are also included in Figure 5(b) and show good agreement with the current data except for G_{IIc} . These values were reported to exhibit significant scatter compared to the values reported in the companion study [21] on mode-II delamination. The companion study adopted recently developed procedures designed to reduce scatter in G_{IIc} , which, in addition to manufacturing procedures, could explain the difference in G_{IIc} seen in Figure 5(b).

R-curves from tests at each mixed-mode ratio are plotted in Figures 6(a) and 6(b). Data in each plot are from all six duplicate tests performed at each mode ratio, excluding all initiation values reported in Table I. The extent of delamination propagation shown is similar to the amount of growth seen in the fatigue tests. The fits

applied to each R-curve (linear fit for $G_{II}/G_I=0.2$ and bi-linear fit for $G_{II}/G_I=0.5$ and 0.8) were used to provide the following relationships between G_R and delamination extension, Δa :

$$G_{R(0.2)} = 1.4195\Delta a + 1.4807$$

$$G_{R(0.5)} = \begin{cases} 3.8549\Delta a + 2.0265 & \Leftarrow 0'' \leq \Delta a \leq 0.119'' \\ 2.485 & \Leftarrow \Delta a > 0.119'' \end{cases} \quad (9)$$

$$G_{R(0.8)} = \begin{cases} 2.7834\Delta a + 2.9480 & \Leftarrow 0'' \leq \Delta a \leq 0.236'' \\ 3.604 & \Leftarrow \Delta a > 0.236'' \end{cases}$$

where $G_{R(0.2)}$, $G_{R(0.5)}$, and $G_{R(0.8)}$ are the delamination resistance at mixed-mode ratios, $G_{II}/G_I=0.2$, 0.5 , and 0.8 , respectively. The open and solid red circles correspond to data used in the linear fits for G_R before the plateau region for $G_{II}/G_I=0.5$ and 0.8 , respectively.

Fatigue Tests

The delamination growth onset data from tests at the three mixed-mode ratios are presented in Figure 7(a). A power law expression is fit to each data set as shown in the figure. The same data are plotted in Figure 7(b) along with the mode-I and mode-II onset curves reported in the companion studies [20, 21]. The parameters of the power law change monotonically with mixed-mode ratio, as shown in Table II. Also, for a given value of G_{max} , the number of cycles required for delamination growth onset increases with increasing mode-II component. This is consistent with the fracture data, which exhibits an increase in G_c with increasing mode-II component (see Figure 5(b)). Lastly, the current data are compared with those from a previous study on IM7/8552 [15] in Figure 8, which shows a reasonable agreement between the two data sets.

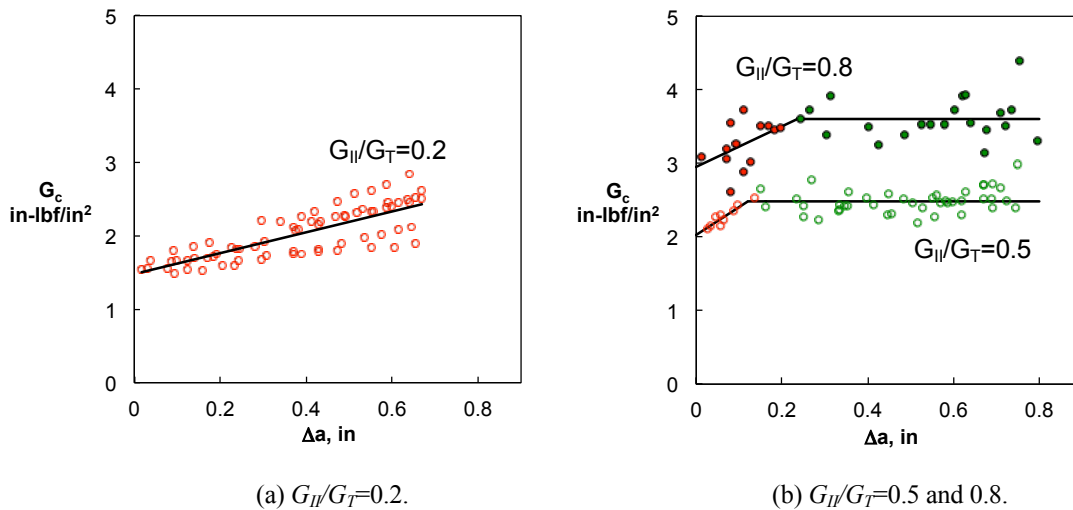


Figure 6 Delamination resistance curves from static tests.

Delamination growth rates from fatigue tests conducted with mixed-mode ratios, $G_{II}/G_T=0.2, 0.5,$ and 0.8 are presented in Figures 9(a), 9(b), and 9(c), respectively, and appear consistent with growth rates reported in the companion studies. The fatigue data from tests conducted at $G_{II}/G_T=0.2$ exhibit an apparent dependence on the value of G_{max} at which a test was started, as shown in Figure 10. The figure presents data from four tests started at the initial load levels indicated. For a given initial load level (bottom-left hand end of each data set), the rate at which growth rate increases tends to decrease with increasing G_{max} . This is consistent with the notion that fiber bridging has more of an effect as the delamination grows. Mode-I tests conducted in the companion study exhibited a very similar effect [20].

Fatigue data of specimens tested at $G_{II}/G_T=0.5$ and 0.8 were relatively insensitive to starting load level, as indicated by the reduced spread in these data sets (see raw data sets in Figures 9(b) and 9(c)). Assuming that the effect of fiber bridging on delamination growth would gradually decrease with an increase in G_{II}/G_T , its influence on the spread in the fatigue data would also be expected to decrease gradually with increasing G_{II}/G_T . However, this is not the case presently because the raw fatigue data from tests conducted at $G_{II}/G_T=0.5$ and 0.8 appear equally insensitive to starting load level (i.e., both exhibit a relatively small spread as seen in Figures 9(b) and 9(c)). However in general, fiber bridging does appear to offer a convincing explanation for the currently observed effect of starting load level on growth rates calculated from the raw data sets.

Normalization affected the fatigue data in a manner that may also be explained by fiber bridging, for three general reasons. First, data from tests involving a mixed-mode ratio, $G_{II}/G_T=0.2$ collapsed after normalization, as was the case in the mode-I delamination companion study [20]. Second, the effect of normalization tended to diminish with increasing mixed-mode ratio, G_{II}/G_T . Third, in the case of $G_{II}/G_T=0.2$, the normalized data tended to yield a faster growth rate for a given G_{max} versus that from the raw data.

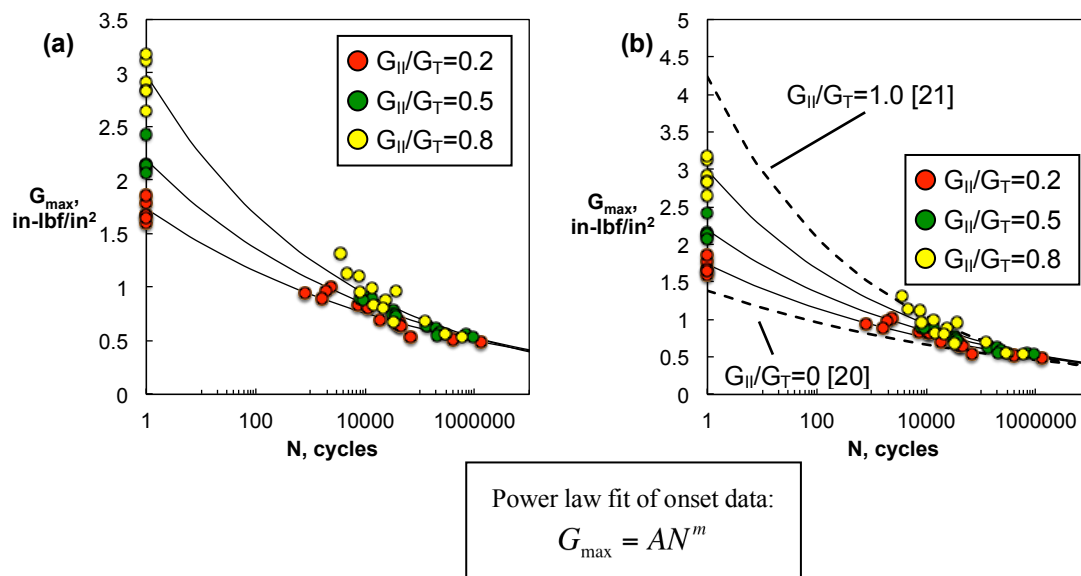


Figure 7 Delamination onset curves (a) MMB data, (b) comparison with companion studies.

Table II Delamination onset power law fit parameters.

G_{II}/G_T	A, in-lbf/in ²	m
0	1.390	-0.080
0.2	1.736	-0.090
0.5	2.189	-0.103
0.8	2.985	-0.125
1.0	4.240	-0.153

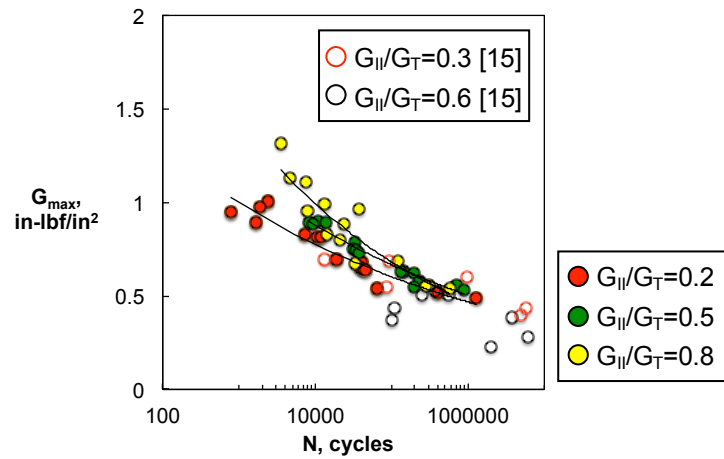


Figure 8 Comparison of growth onset between current data sets and previous results [15].

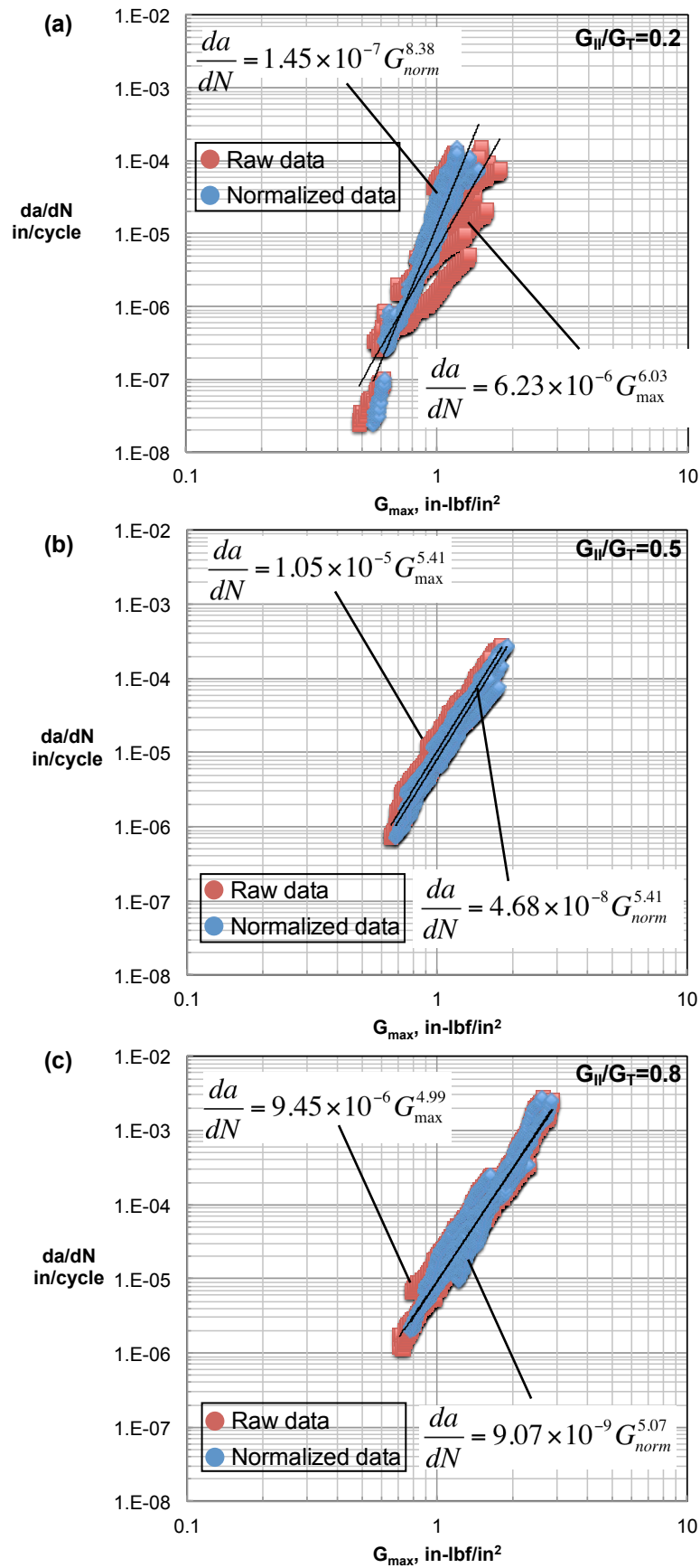


Figure 9 Delamination growth rates (a) $G_{II}/G_I=0.2$, (b) $G_{II}/G_I=0.5$, (c) $G_{II}/G_I=0.8$.

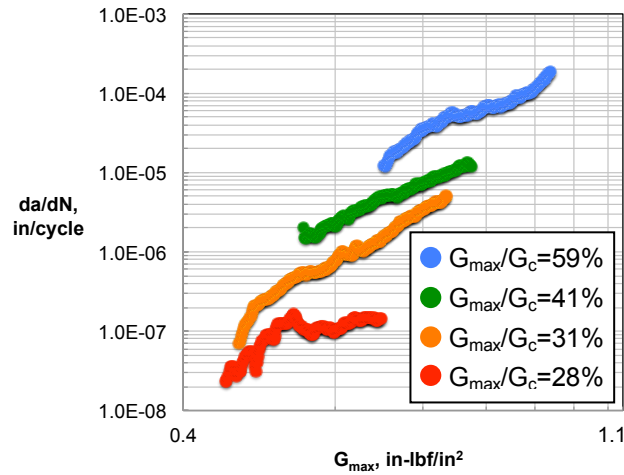


Figure 10. Fatigue data from tests conducted at $G_{II}/G_T=0.2$.

As was expected from the growth onset data (see Figure 7(b)), the Paris law exponent, n , generally exhibited a monotonic decrease with increasing G_{II}/G_T , based on the raw fatigue data (see Figure 11(a) and Table III). This result is consistent with the onset data because a monotonic increase in fracture toughness with increasing G_{II}/G_T should tend to decrease the Paris law exponent. The normalized data, however, do not exhibit this monotonic behavior (Note that pure mode II fatigue data were not normalized, see Figure 11(a)). In this case, normalization yielded a decrease in n during the pure mode I tests, whereas it resulted in an increase in n during the mixed-mode tests conducted at $G_{II}/G_T=0.2$. The reason for this differing effect of normalization on n is due to the control mode used in the two test types. The pure mode-I tests of the companion study were conducted using *displacement*-controlled constant amplitude cycling [20]. An example data set from this testing series is presented in Figure 12(a) (initial $G_{I_{max}}=0.37G_{Ic}$). The beginning of the test corresponds to the upper-right quadrant of the plot. As delamination growth occurs G_{max} decreases and G_R increases (a relationship between G_R and delamination growth similar to that shown in Figure 6(a) was reported [20]). Consequently, the fatigue data in Figure 12(a) rotate clockwise when normalized, yielding a reduction in Paris law exponent. Conversely, the mixed-mode tests in this study were conducted using load-controlled constant amplitude cycling (see example data set in Figure 12(b)). In this case the beginning of the test corresponds to the lower-left quadrant of the plot. As delamination growth occurs both G_{max} and G_R increase. Consequently, the fatigue data rotate counterclockwise when normalized, yielding an increase in the Paris law exponent (Figure 12(b)).

In the case of the Paris law coefficient, D , (see Figure 11b) the normalized data yield a monotonic change in this parameter with G_{II}/G_T , whereas the raw data do not. Interestingly, however, the Paris law parameters do vary monotonically with G_{II}/G_T if data only from the mixed-mode tests are considered. In this case, a trend can be defined within the limit: $0.2 \leq G_{II}/G_T \leq 0.8$.

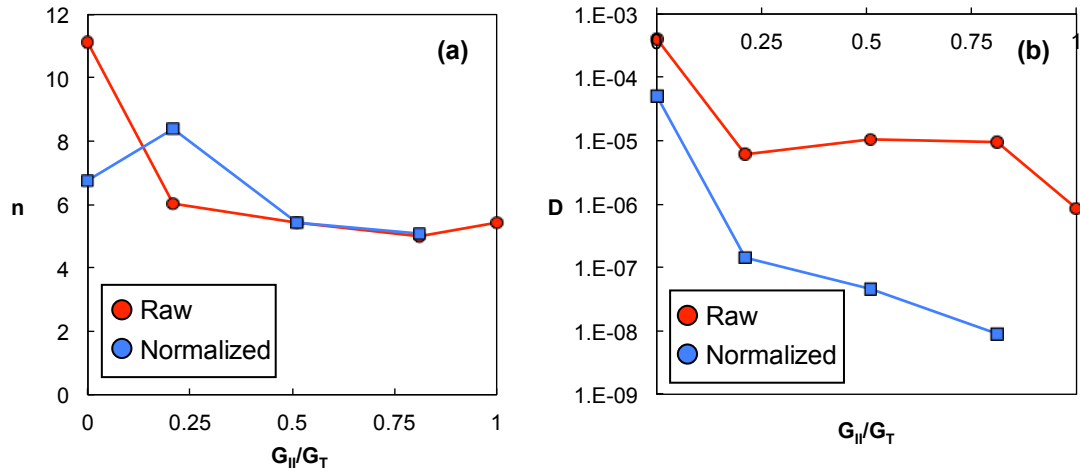


Figure 11 Effect of mixed-mode ratio on Paris law parameters (a) Paris law exponents, (b) Paris law coefficients.

TABLE III. Paris law parameters for different mixed-mode ratios

G_{II}/G_T	D	n	D (norm)	n (norm)
0	$4.00E-04$	11.15	$5.16E-05$ [20]	6.77 [20]
0.2	$6.23E-06$	6.03	$1.45E-07$	8.38
0.5	$1.05E-05$	5.41	$4.68E-08$	5.41
0.8	$9.45E-06$	4.99	$9.07E-09$	5.07
1	$8.64E-07$ [21]	5.45 [21]	N/A	N/A

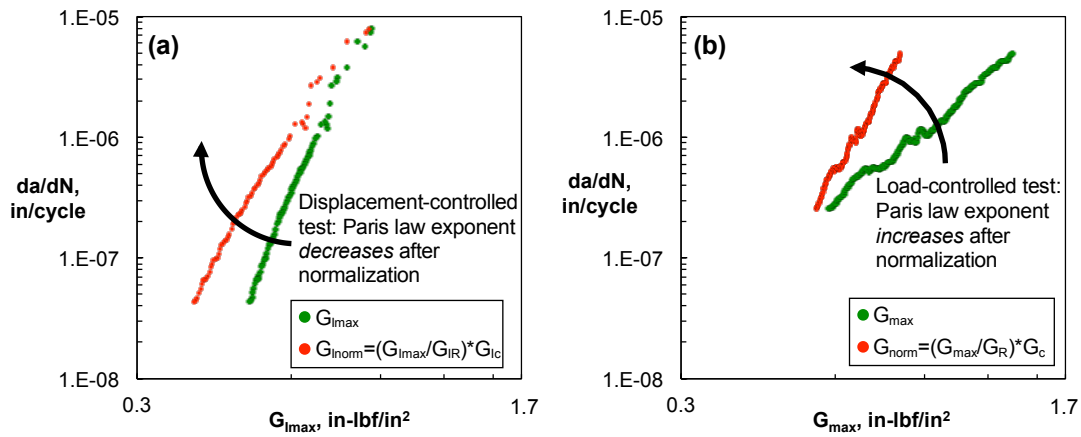


Figure 12 Effect of normalization (a) Mode-I fatigue data, (b) Mixed mode fatigue data ($G_{II}/G_I=0.2$)

SUMMARY

Mixed-mode bending tests were conducted at three different mixed-mode ratios as part of a study to characterize the fatigue and fracture (delamination) behavior of IM7/8552 graphite/epoxy tape. The following general observations were made:

- Static tests yielded a delamination initiation criterion that is consistent with existing data from the literature.
- Fatigue delamination onset behavior varied monotonically with mixed-mode ratio, G_{II}/G_T , as was expected based on the condition that $G_{IIc} > G_{Ic}$.
- In specimens tested at $G_{II}/G_T=0.2$, delamination growth rates tended to be affected by starting load level consistently with the notion that the effect arises from fiber bridging.
- Specimens tested at $G_{II}/G_T=0.5$ and 0.8 exhibited little sensitivity to initial load level compared to specimens tested at $G_{II}/G_T=0.2$.
- Normalization using the static R-curve only affected fatigue data from tests conducted at $G_{II}/G_T=0.2$. In this case, normalization almost eliminated any apparent effect of initial load level on growth rates. This is again consistent with the notion that the effect of initial load level on growth rate is caused by fiber bridging.
- Paris law exponent, n , based on the raw fatigue data sets exhibited a monotonic decrease with increasing G_{II}/G_T , as expected based on the fracture toughness data. This was not the case for the normalized data.
- Paris law coefficient, D , based on the raw fatigue data sets did not follow a monotonic change with respect to G_{II}/G_T , whereas that based on the normalized data does vary monotonically.
- Both Paris law parameters exhibit monotonic changes with respect to G_{II}/G_T in the mixed-mode range of $0.2 \leq G_{II}/G_T \leq 0.8$.

In general, the fatigue behavior of the material tested changes with mixed-mode ratio, G_{II}/G_T , in a manner that is consistent with fatigue behavior during purely mode-I and mode-II loading conditions (i.e., growth rates tend to decrease with increasing mode-II loading). In addition, delamination growth rates do seem to be affected by fiber bridging that is typically associated with unidirectional laminates, and this effect does diminish with an increase in G_{II}/G_T . This is expected considering that bridging fibers would be expected to yield a reduced influence over growth rates under increasing mode-II loading conditions.

REFERENCES

1. O'Brien, T.K. 1982. "Characterization of delamination onset and growth in a composite laminate," *Damage in Composite Materials*, ASTM STP 775, K. L. Reifsnider, Ed., American Society for Testing and Materials, Philadelphia, pp. 140-167.
2. Pipes, R. Byron, and N.J. Pagano. 1970. "Interlaminar stresses in composite laminates under uniform axial extension," *J. Comp. Mats*, 4(4): 538-548.
3. Asp L.E., A. Sjögren, E.S. Greenhalgh. 2001. "Delamination growth and thresholds in a carbon/epoxy composite under fatigue loading," *J Compos Technol Res*; 23(2): 55–68.
4. Wilkins D.J. et al. 1982. "Characterizing delamination growth in graphite-epoxy," ASTM STP 775, K. L. Reifsnider, Ed., American Society for Testing and Materials, Philadelphia, 168–83.
5. "ASTM D 5528-13, Standard Test Method for Mode I Interlaminar Fracture Toughness of Unidirectional Fiber-Reinforced Polymer Matrix Composites," in *Annual Book of ASTM Standards*. Vol. 15.03, ASTM International, 2014.
6. "ASTM D 6671- D 6671M-(04)13, Standard Test Method for Mixed Mode I-Mode II Interlaminar Fracture Toughness of Unidirectional Fiber-Reinforced Polymer Matrix Composites," in *Annual Book of ASTM Standards*. Vol. 15.03, ASTM International, 2014.

7. "ISO/FDIS 15114, Fibre-Reinforced Plastic Composites - Determination of the Mode II Fracture Resistance for Unidirectionally Reinforced Materials Using the Calibrated End-Loaded Split (C-ELS) Test and an Effective Crack Length Approach," *International Standards Organization*, Technical Committee 61, 2014.
8. "ASTM Draft Standard, WK22949, Standard Test Method for Determination of the Mode II Fracture Toughness of Unidirectional Fiber-Reinforced Polymer Matrix Composites," ASTM International Subcommittee on Interlaminar Properties, D30.06, 2014.
9. "ASTM D 6115-(97)14, Standard Test Method for Mode I Fatigue Delamination Growth Onset of Unidirectional Fiber-Reinforced Polymer Matrix Composites," in *Annual Book of ASTM Standards*. Vol. 15.03, ASTM International, 2014.
10. Matsubara G, H. Ono, and K. Tanaka. 2006. "Mode II fatigue crack growth from delamination in unidirectional tape and satin-woven fabric laminates of high strength GFRP," *Int J Fat.* 28: 1177–86.
11. Martin, R.H., and G.B. Murri. 1990. "Characterization of Mode I and Mode II Delamination Growth and Thresholds in AS4/PEEK Composites," *Composite Materials: Testing and Design (Ninth Volume)*, ASTM STP 1059, S. P. Garbo, Ed., American Society for Testing and Materials, Philadelphia, pp. 251-270.
12. Kenane M. 2009. "Delamination growth in unidirectional glass/epoxy composite under static and fatigue loads," *Phys Proc.*, 2(3):1195–203.
13. Lin CT, P.W., Kao. 1996. "Delamination growth and its effects on crack propagation in carbon fiber reinforced aluminum laminates under fatigue loading," *Acta Mater.*, 44(3):1181–8.
14. Lin CT, P.W., Kao. 1996. "Fatigue delamination growth in carbon fibre-reinforced aluminium laminates," *Comp. Part A* 27:9–15.
15. Hansen, P., and R., Martin. 1999. "DCB, 4ENF and MMB delamination characterisation of S2/8552 and IM7/8552," Materials Engineering Research Lab Report. European Research Office of the US Army.
16. Kenane, M., and M.L. Benzeggagh. 1997. "Mixed-mode delamination fracture toughness of unidirectional glass/epoxy composites under fatigue loading," *Comp. Sci. Tech.*, 57(5): 597-605.
17. Schön, J. 2000. "A model of fatigue delamination in composites," *Comp. Sci. Tech.*, 60(4): 553-558.
18. Blanco, N., E.K. Gamstedt., L.E. Asp, and J. Costa. 2004. "Mixed-mode delamination growth in carbon–fibre composite laminates under cyclic loading," *Int. J. Sol. Struc.*, 41(15): 4219-4235.
19. Rans, C., R. Alderliesten, and R. Benedictus. 2011. "Misinterpreting the results: How similitude can improve our understanding of fatigue delamination growth," *Comp. Sci. Tech.* 71(2): 230-238.
20. Murri, G.B. 2013. "Evaluation of Delamination Onset and Growth Characterization Methods Under Mode I Fatigue Loading," National Aeronautics and Space Administration Technical Memorandum, NASA/TM-2013-0010557.
21. O'Brien, T.K., W.M. Johnston, and G. J. Toland. 2010. "Mode II interlaminar fracture toughness and fatigue characterization of a graphite epoxy composite material," National Aeronautics and Space Administration Technical Memorandum, NASA/TM-2010-216838.
22. Nakai, Y. and C. Hiwa. 2002. "Effects of Loading Frequency and Environment on Delamination Fatigue Crack Growth on CFRP," *Int. J. Fat.* 24: 161-170.
23. Fracture Technology Associates, Bethlehem, PA. <http://www.fracturetech.com/index.html>
24. O'Brien, T.K. and R. Krueger. 2003. "Analysis of Flexure Tests for Transverse Tensile Strength Characterization of Unidirectional Composites," *J Compos Technol Res*, 25: 50-68.
25. ASTM E 647-00, "Standard Test Method for Measurement of Fatigue Crack Growth Rates," in *Annual Book of ASTM Standards*. Vol. 03.01 ASTM International, 2014.
26. P.C. Paris, M.P. Gomez and W. E. Anderson. 1961. "A Rational Analytic Theory of Fatigue," *The Trend in Engineering*, 13: 9-14.
27. Poursartip, A., 1987. "The Characterization of Edge Delamination Growth in Laminates Under Fatigue Loading," *Toughened Composites*, ASTM STP 937, Norman J. Johnston, Ed., American Society for Testing and Materials, Philadelphia, pp. 222-241.
28. Shivakumar, K., H. Chen, and F. Abali. 2006. "A Total Fatigue Life Model for Mode I Loaded Composite Laminates," *Int. J. Fat.* (28)1: 33-42.

29. Murri, G. and N.V. De Carvalho. "A novel method for characterizing fatigue delamination growth under Mode I using the Double Cantilever Beam specimen," Proceedings of the American Society for Composites – Twenty-eighth Technical Conference, San Diego, CA, USA, paper 658.
30. Davidson, B.D., "Interlaboratory Study to Establish Precision Statements for ASTM WK22949, New Standard Test Method for Determination of the Mode II Interlaminar Fracture Toughness of Unidirectional Fiber Reinforced Polymer Matrix Composites Using the End-Notched Flexure (ENF) Test," ASTM Research Report, 2012.
31. O'Brien, T.K. 1998. "Composite Interlaminar Shear Fracture Toughness: G_{IIc} : Shear Measurement or Sheer Myth?" *Composite Materials: Fatigue and Fracture, Seventh Volume, ASTM STP 1330*, R.B. Bucinell Ed., American Society for Testing and Materials, Philadelphia, pp. 3-18.